Journal of Materials Chemistry A

Accepted Manuscript

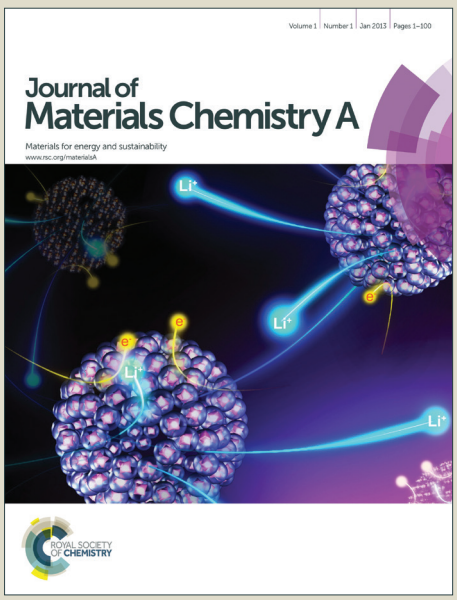

ROYAL SOCIETY OF CHEMISTRY

www.rsc.org/materialsA

Graphical Abstract

A simple and effective protocol was presented to fabricate SnO_2/carbon/graphene (SnO_2/C/GN) nanocomposites with different compositions and nanostructures. SnO_2/C/GN-1.5 with only 1.5 wt% GN shows a stable capacity at 720 mAh g^{-1} after 70 cycles, which is ascribed to the synergetic effects of a unique combination of material properties.

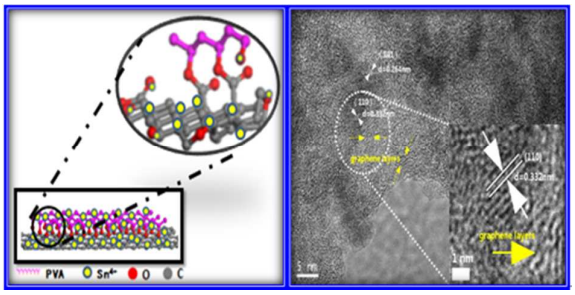

Journal Name

RSCPublishing

ARTICLE

Graphene Enhanced Carbon-Coated Tin Dioxide Nanoparticles for Lithium-ion Secondary Battery†

Cite this: DOI: 10.1039/xoxxoooooox

Zhongtao Li,‡ Guiliang Wu,‡ Dong Liu, Wenting Wu, Bo Jiang, Jingtang Zheng, Yanpeng Li, Junhua Li, Mingbo Wu*

Received ooth January 2012,
Accepted ooth January 2012

DOI: 10.1039/xoxxoooooox

www.rsc.org/

A one-step, scale-upable method has been developed to prepare SnO_2 based carbon materials. Their performances as anode for lithium-ion battery can be improved through simultaneous growth of SnO_2 nanoparticles, a carbonaceous polymer coating and "doping" of graphene oxide (GO) by thermal treatment. Detailed characterizations of the resulting composite materials using transmission electron microscopy and X-ray diffraction suggest that "doping" certain amount GO could obviously change the crystallinity and distribution of SnO_2 nanoparticles in the mixture. The SnO_2 based carbon material exhibits stable reversible capacity at 720 mAh g^{-1} after 70 cycles as the anode of lithium-ion batteries, indicating that the composites might have a promising future as application in Li-ion batteries.

1. Introduction

Lithium-ion secondary batteries (LIBs) are playing essential role for electronic devices in the modern world, such as communication devices, portable devices, and electrical/hybrid vehicles. Even though LIBs have many advantages like high electromotive force and high energy density, the requirements on their specific capability, charging stability and rate capability are increasing with the development of technology. Many research attempts have been made to explore new electrode materials or design novel nanostructures of electrode materials to meet the new demands.[1-3] For an anode material in LIBs, graphite is usually employed as a standard electrode because it can be reversibly charged and discharged under intercalation potentials with reasonable specific capacity.[4] To increase battery's capability, some elements or compounds (*e.g.* Sn, Sb, Si or Ge) alloyed lithium with much larger specific capacities than commercial graphite are adopted to replace carbon-based anode.[5-8]

Among these studies, the electrochemical reactivity of SnO_2 has drawn much attention, due to its high theoretical capacity (782 mAh g^{-1}) during cyclic process.[9,10] And, the tin dioxide anode has higher operating voltage than graphite, so the safety of batteries during rapid charge/discharge cycle could be improved.[11] However, the practical uses of the tin oxide materials are restricted, because they suffer severe volume variation (around 300%) during Li^+ insertion and extraction. This effect often causes electrode disintegration and rapid capacity fading.[12] To solve these problems, various nanostructured SnO_2 and SnO_2 composites have been proposed with the aim of stabilizing the active electrode material by accommodating the volume change during cyclic process.[13,14] Metal oxide particles with small size and homogeneous carbon coating have already been reported to improve the mechanical stability and the electrochemical performances because of the buffering effect and low activity of the carbon coating.[15,16] An electrochemical improvement in the performances of the SnO_2/carbon nanocomposites is achieved due to the role of the carbon support which enables a better accommodation of the large volume change and improves the electron conductivity of the electrode.[17]

As have been reported previously, glucose, sucrose and some other water soluble polysaccharides as the widely used precursors were carbonized by thermal treatment to form carbon matrix for tolerating SnO_2 nanocrystal.[9,18] However, the capacity retention of some reported carbon-coated materials is still limited, which mainly arises from the relative inhomogeneous nanoparticles and low conductivity of coated carbon.[19,20] Moreover, some of previous methods for producing carbon-coated materials were relatively complicated and the core-shell nanostructure was usually obtained in a multistep approach.[21,22] Thus it has remained a challenge to find an approach that can simultaneously ensure both the homogeneous dispersion of SnO_2 nanoparticles (NPs) and the construction of conductive carbon matrix.

Graphene (GN) also has recently been investigated as the functional matrix support for SnO_2-based nanostructures due to its intrinsic properties of flexible two-dimensional structure, high surface area (over 2600 m^2 g^{-1}) and excellent electrical conductivity, which not only facilitate the transfer of electrons and the transport of electrolyte in the electrode, but also diminish the stress of the collective electrode upon battery cycling.[23,24] However, the SnO_2-based nanoparticles could be easily peeled off from the graphene and afterwards pass through the pores of the separator, and finally agglomerate on the anode, leading to self-discharge, capacity loss and even electrode failure.[25] Meanwhile, for the cost control of practically application, the content of more expensive GN in the materials should be kept in a reasonable level. Therefore, it is greatly important to develop a facile and reliable approach to synthesize

desirable nanocomposites that can reliably bind SnO_2-based nanostructures with graphene to avoid such issues.

In order to overcome these problems, many kinds of SnO_2/Carbon composites for LIBs had been reported, most of which adopted a great amount of GN to form the supporting matrix or multistep approaches.[26-28] Few SnO_2/C/GN composite also have been published: Liang and co-workers reported a SnO_2-polyaniline-reduced graphene oxide anode in LIBs which presents discharge capacities 574 mAh g^{-1} after 50 cycles, which corresponds to 74 % of its theoretical specific capacity.[29] Li and co-workers reported SnO_2–carbon–RGO with 862 mAh g^{-1} of specific discharge capacity in the initial cycle and 622 mAh g^{-1} after 100 cycles.[30] Zhang and co-workers reported a carbon-coated SnO_2/graphene nanosheets, which presents an initial capacity of 1310 mAh g^{-1} and 757 mAh g^{-1} can be retained after 150 cycles, which contains 10 wt% graphene in the composite.[31]

Herein, we have attempted to prepare homogeneous carbon coated SnO_2 NPs in the presence of graphene. Polyvinyl alcohol (PVA), which could be considered as surface-active agent to help forming homogeneous SnO_2 particles and could effectively transfer to covalent framework at high temperature, was adopted as starting carbon material and followed by thermal treatment to fabricate less active carbon substrate to mitigate the volume change during cycling. Small amount of graphene was also involved simultaneously to facilitate the transfer of electrons and the transport of electrolyte in the electrode. After hydrothermal treatment with cheap starting materials, *i.e.* polyvinyl alcohol, graphene oxide, stannic chloride and ammonia, carbon-coated SnO_2 NPs were obtained. When used as anode materials in LIBs, the graphene enhanced carbon-coated SnO_2 nanoparticles exhibit significantly improved cycling performance as compared to carbon-coated SnO_2 NPs without graphene. The result demonstrates that suitable graphene could effectively improve the cycling performance of the SnO_2-based anode materials in LIBs.

2. Experimental

2.1. Preparation of SnO_2/C composites

In a typical synthesis of the composites, polyvinyl alcohol was gradually added in deionized water (65 mL) along with stirring and then slowly heated to 85 °C for absolute dissolution in a water bath. The above solution was denoted as solution B. Tin (IV) chloride pentahydrate ($SnCl_4{\cdot}5H_2O$) was dissolved to the solution of 60 mL distilled water and 1 mL appropriate concentrated hydrochloric acid under stirring. The obtained solution was labelled as solution C.

Solutions B and C were completely mixed, and its pH value was adjusted among 9-10 by injecting amounts of ammonium hydroxide (25.0-38.0 wt%). The above mixture was stirred sufficiently in a water bath for 1 h at 85 °C and then dried at 100 °C for 24 h. Finally, the SnO_2/C composite was gained after calcinating in a tube furnace under high-purity N_2 at 500°C for 2 h. The as-prepared samples were denoted as SnO_2/C. The contents of SnO_2 in different samples are calculated by the following formula:

$$\boldsymbol{SnO_2}\% = \frac{m_{SnO_2}}{(m_{PVA}+m_{SnO_2})}$$

According to the formula, SnO_2% of SnO_2/C-10, SnO_2/C-30 and SnO_2/C-50 are 10%, 30% and 50%, respectively.

2.2. Preparation of SnO_2/C/GN composites

Graphite oxide was first synthesized from graphite powder by a modified Hummers' method.[32] Graphite oxide (100 mg) was exfoliated in distilled water (100 mL) with ultrasonic treatment (700 W, 1 h) to form a colloidal suspension, and the resultant suspension was marked as solution A. As mentioned above, solutions B and C were prepared and mixed. Solution A was slowly injected into the mixture of solutions B and C. Finally, the SnO_2/C/GN composite was obtained via the same process of SnO_2/C. The content of GN in different samples can be approximately estimated by the following equation:

$$\boldsymbol{GN}\% = \frac{m_{GO}}{(m_{PVA}+m_{SnO_2}+m_{GO})}$$

According to the formula, the samples containing 0.7%, 1.5%, 5%, 10% and 15% GN are labelled as SnO_2/C/GN-0.7, SnO_2/C/GN-1.5, SnO_2/C/GN-5, SnO_2/C/GN-10, and SnO_2/C/GN-15, respectively.

For comparison, the control samples of pure SnO_2, C/GN (carbonized PVA with 1.5 wt% graphene) and SnO_2/GN (50 wt% SnO_2 coated by graphene) were synthesized by the same method as mentioned above.

2.3. Sample characterization

The structures and morphologies of the SnO_2/C and SnO_2/C/GN nanocomposites were characterized by X-ray diffraction (XRD) (X'Pert PRO MPD, Holland), field emission scanning electron microscopy (FE-SEM) (Hitachi S-4800, Japan), and transmission electron microscopy (TEM) (JEM-2100UHR, Japan). The functional groups in SnO_2/C and SnO_2/C/GN were characterized by Fourier transform infrared spectrometry (FTIR) (Thermo Nicolet NEXUS 670, USA). The thermal properties and the compositions of the samples were characterized by thermogravimetric analysis (TGA) (STA 409 PC Luxx, Germany).

2.4. Electrochemical measurements

As-prepared SnO_2 based carbon materials were mixed with carbon black and poly(vinylidene) fluoride (PVDF) binder (80: 10: 10 in weight ratio) in *N*-methyl-2-pyrrolidinone (NMP) to form a homogeneous slurry, which was then coated onto a copper foil current collector to prepare the working electrode. The prepared working electrode was dried in a vacuum oven at 100 °C for 10 h and then assembled into a half-battery in an Ar-filled glove box. Half-battery (CR2032 coin type) was manufactured by employing the SnO_2 based carbon material as working electrode, Li foil as the counter electrode and reference electrode, a microporous polypropylene film as the separator, and 1 mol L^{-1} $LiPF_6$ in a 1:1 (v/v) mixture of ethylene carbonate(EC) and dimethyl carbonate (DMC) as the electrolyte. The cells were galvanostatically charged-discharged in the potential range 0.005-2.5 V *vs.* Li/Li^+ at the current density of 100, 200, 400 and 800 mA g^{-1} on a Land CT2001A cycler. Cyclic voltammograms (CV) were performed using an Ametek PARSTAT4000 electrochemistry workstation at 0.25 mV s^{-1} within the potential range of 0.01-2.5 V.

3. Results and Discussion

XRD patterns of SnO_2/C/GN-1.5 and SnO_2/GN are shown in Fig. 1. The peak of GO at 11.4° (see Fig. S1(c)), which represents the weak

van der Waals force between layers of GO, could not be identified in Fig. 1(a) because of the small amount addition of GO, the disordered stacking characteristics of the graphene sheets and the disordered nature of the carbon.[33,34] The higher angle peak of sample C/GN in Fig. S1(b) of the d3 spacing at 25.5° corresponds to a distance of approximate 3. 49 Å that can be assigned to the π-π stacking between aromatic rings. The four dominant broad peaks (110), (101), (211), and (301) are attributed to the SnO_2 phase (JCPDS No. 41-1445), indicating the formation of tetragonal SnO_2 nanocrystal.

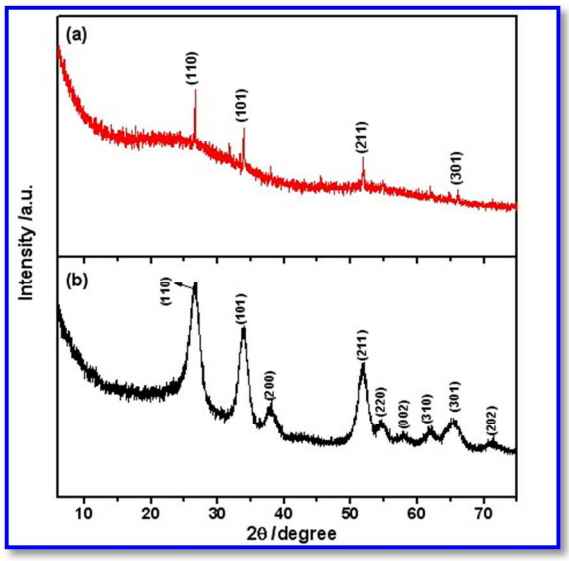

Fig. 1 XRD patterns of (a) SnO_2/C/GN-1.5 and (b) SnO_2/GN

These diffraction peaks in SnO_2/C/GN-1.5 are obviously stronger than those of SnO_2/C-50 (see Fig. S1(a)), which suggest the higher crystallinity due to the introduction of GO. In all cases, the peak of carbon couldn't be identified, which reveals the amorphous carbon in the mixture. The XRD pattern of SnO_2/GN in Fig. 1(b) is similar to SnO_2/C/GN-1.5. The four dominant broad peaks (110), (101), (211), and (301) are attributed to the SnO_2 phase, which are stronger and broader than those of SnO_2/C/GN-1.5. It indicates that the tetragonal SnO_2 nanocrystals are well formed through the help of crystalline GN.

As shown in Fig. 2, FTIR spectrum of carbonized PVA (C-PVA) shows the stretching vibrations of C=C and aromatic cycles around 1580 cm^{-1} and the strong transmission from 900 cm^{-1} to 600 cm^{-1} could be signed as finger print region of C-H on aromatic cycle.[35,36] The injection of Sn^{4+} ion into PVA and high temperature treatment introduce a strong peak at 580 cm^{-1}, which is ascribed to Sn-O in the curve of SnO_2/C and the mentioned peaks on C-PVA could also be identified. After the addition of GO in the mixture, as shown in profile SnO_2/C/GN, the thermal treatment eliminates most of oxygen-containing groups on GO such as COOH peaks (1735 cm^{-1}), C-O stretching vibrations (1052 cm^{-1}), O-H deformation peak (1401 cm^{-1}) and O-C=O peak (827 cm^{-1}), which indicates that GO has been reduced to graphene in some degree. The transmission curves of SnO_2/C/GN are almost the same as those of SnO_2/C except a new peak at 640 cm^{-1}, which might come from the aromatic cycles. The introduction of GN seems to play some positive role on aromatization during the thermal carbonization. The FT-IR spectra of graphite oxide and SnO_2 are shown in Fig. S2.

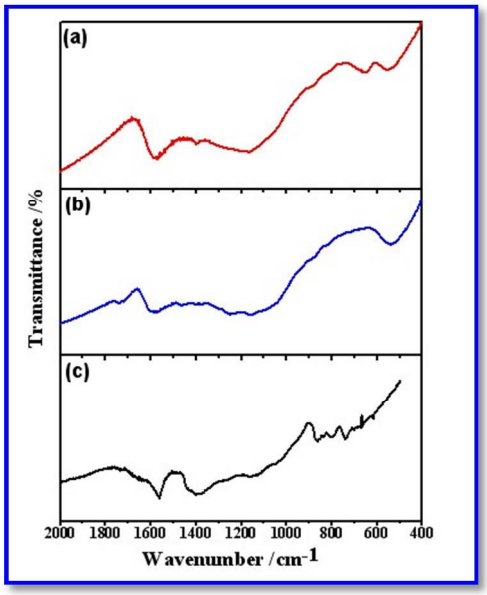

Fig. 2 FT-IR spectra of (a) SnO_2/C/GN-1.5, (b) SnO_2/C-50 and (c) C-PVA

In order to assess the thermal property and the composition of SnO_2/C/GN-1.5, thermogravimetric analysis (TGA) is employed in air. As shown in Fig. 3, the first major weight loss (about 6%) in the range of 40-150 °C corresponds to the removal of absorbed H_2O. It is revealed that a significant weight loss takes place at 300-600 °C, which should be attributed to the combustion of amorphous carbon and graphene. Finally, only SnO_2 NPs could be left. Based on weight loss in the TGA curve, the SnO_2 content in SnO_2/C/GN-1.5 could be estimated, *i.e.* 42%, which is relatively lower than 50% of calculated value. This variation may originate from addition of graphene oxide, absorbed water and decomposition of products in the followed thermal treatment.

The morphologies of SnO_2/C/GN-1.5 and SnO_2/C-50 samples are studied by field emission transmission electronic microscopy (TEM) in Fig. 4. In Fig. 4(a), SnO_2/C/GN-1.5 is formed by bulk carbon particles with SnO_2 NPs homogeneously dispersed inside them (darker dots). In Fig. 4(b), high-resolution (HR) TEM image of SnO_2/C/GN-1.5 is presented and the lattice fringes of SnO_2 NPs are clearly visible (see insert). The interlayer spacings are about 0.33 nm

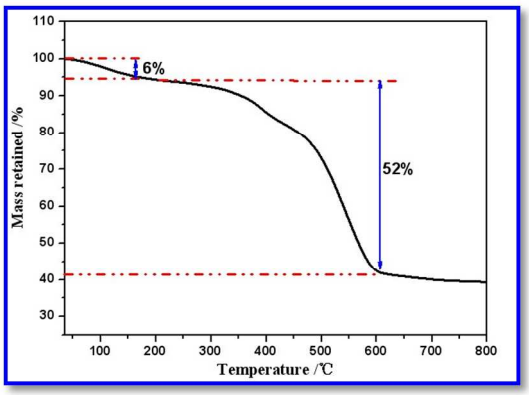

Fig. 3 TGA curve of SnO_2/C/GN-1.5 in air

and 0.26 nm respectively corresponding to (110) and (101) planes of SnO_2. Thin layers of carbon in form of stacked graphene sheets can be found on the edges of SnO_2 particles (*cf.* arrows). Therefore, the

SnO_2 NPs are wrapped between the graphene sheets and the amorphous carbon coating layers, which provides a perfectly conductive carbon network, facilitating electron transfer, buffering the volume changes, preventing the aggregation of SnO_2 NPs, and maintaining the contact between graphene sheets and SnO_2 NPs during Li^+ insertion/extraction, thus improving the electrochemical performance as an anode material for LIBs. SnO_2 NPs also disperse well in SnO_2/C-50 as described in Figs. 4(c) and 4(d), and some SnO_2 nanocrystals could be identified. It is noted that the sizes of SnO_2 nanocrystals are somewhat larger than those in SnO_2/C/GN-1.5, and most SnO_2 still exist in amorphous state, which have been proved in XRD. The TEM images of control sample SnO_2/GN are shown in Figs. S4(a) and 4(b). The SnO_2 nanocrystals are distributed uniformly on the surface of GN and the size are smaller than those in SnO_2/C/GN-1.5, which have also been approved by XRD. The GN conjugated planes seem to have some special interaction with SnO_2, which could help the growth and distribution of SnO_2 nanocrystals. In sample C/GN (see Fig. S4(c)), structures in crystalline manner could not be identified, which reveal the amorphous carbon in the composite.

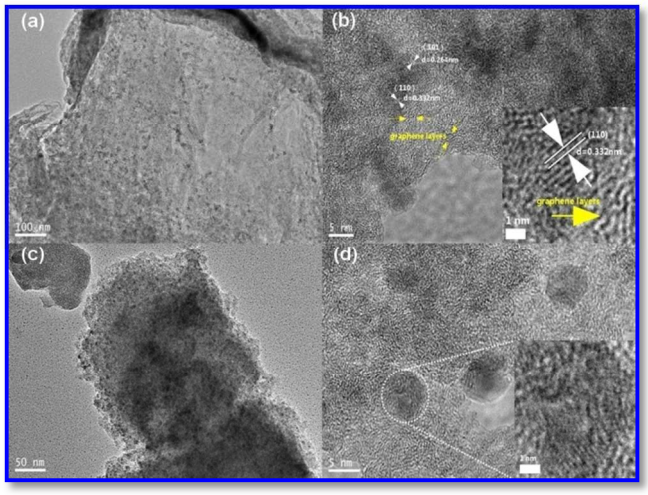

Fig. 4 TEM images of (a) SnO_2/C/GN-1.5, (c) SnO_2/C-50 and HRTEM images of (b) SnO_2/C/GN-1.5, (d) SnO_2/C-50

Field emission scanning electron microscopic (FE-SEM) images in Fig. S3 show that SnO_2/C-50 and SnO_2/C/GN-1.5 have almost uniform morphology over large domains. Both SnO_2/C-50 and SnO_2/C/GN-1.5 can be imaged well without Au coating, which suggests that the obtained samples possess good electrical conductivities. The high resolution images give the distribution details of SnO_2 NPs on the surface of amorphous carbon (Figs. S3(a) and (b)). In all cases, the SnO_2 NPs are distributed on the carbon matrix. SnO_2 NPs in SnO_2/C-50 are with a diameter of about 50 nm and a little larger in SnO_2/C/GN-1.5, both of which covered by a carbon layer.

The involvement of GO seems to not only increase the crystallinity of SnO_2, but also avoid particles agglomeration. Based on the experiment data, we propose a possible mechanism for material manufacturing (Fig. 5). Initially, most injected Sn^{4+} interact with –OH groups on the PVA chains, which could be considered as surfactant. When GO with many oxygen-containing groups is added to above mixture, the formation of interfacial bonds between graphene oxide sheets and PVA molecules interacted with Sn^{4+} NPs are propitious to the stabilization of SnO_2 NPs decorating on graphene oxide sheets. During the following assembling process, SnO_2 nanocrystals could grow up in higher crystalline size and the

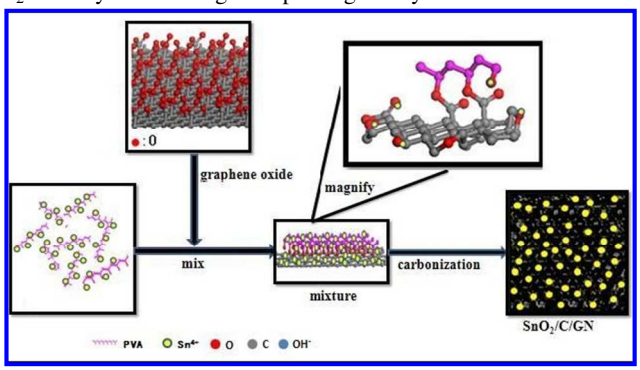

Fig. 5 Synthesis schematic and the structure of SnO_2/C/GN

voids existing between individual composite sheets could be fixed by carbonized PVA for stabilization. Graphene oxide sheets act as crystal nucleuses for promoting the growth and distribution of SnO_2 nanocrystals, which have been approved by XRD and TEM.

To evaluate the abilities of SnO_2 based carbon materials in Li^+ storage, the samples are used as the anodes for LIBs. The first two cycles for charge/discharge properties of three graphene-free samples (SnO_2/C-10, SnO_2/C-30 and SnO_2/C-50) at 100 mA g^{-1} of current density and a voltage cut-off of 2.5/0.005 V versus Li/Li^+ are shown in Fig. 6. As shown in Fig. 6(a), with the increasing SnO_2, the capacities of the first discharge/charge are increased simultaneously, which are 443/427, 984/710 and 1267/924 mAh g^{-1}, respectively.

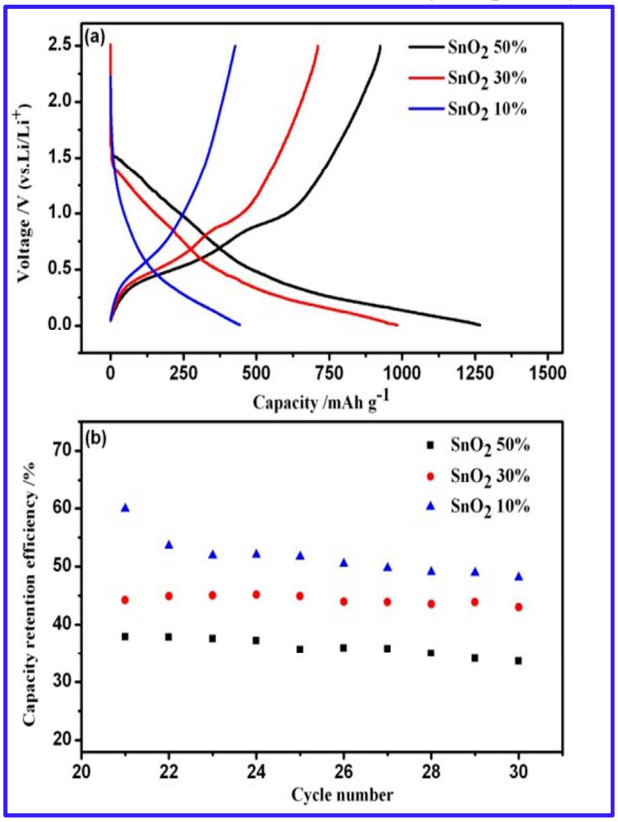

Fig. 6 (a) Charge/discharge profiles and (b) capacity retention efficiency profiles of SnO_2/C-10, SnO_2/C-30 and SnO_2/C-50

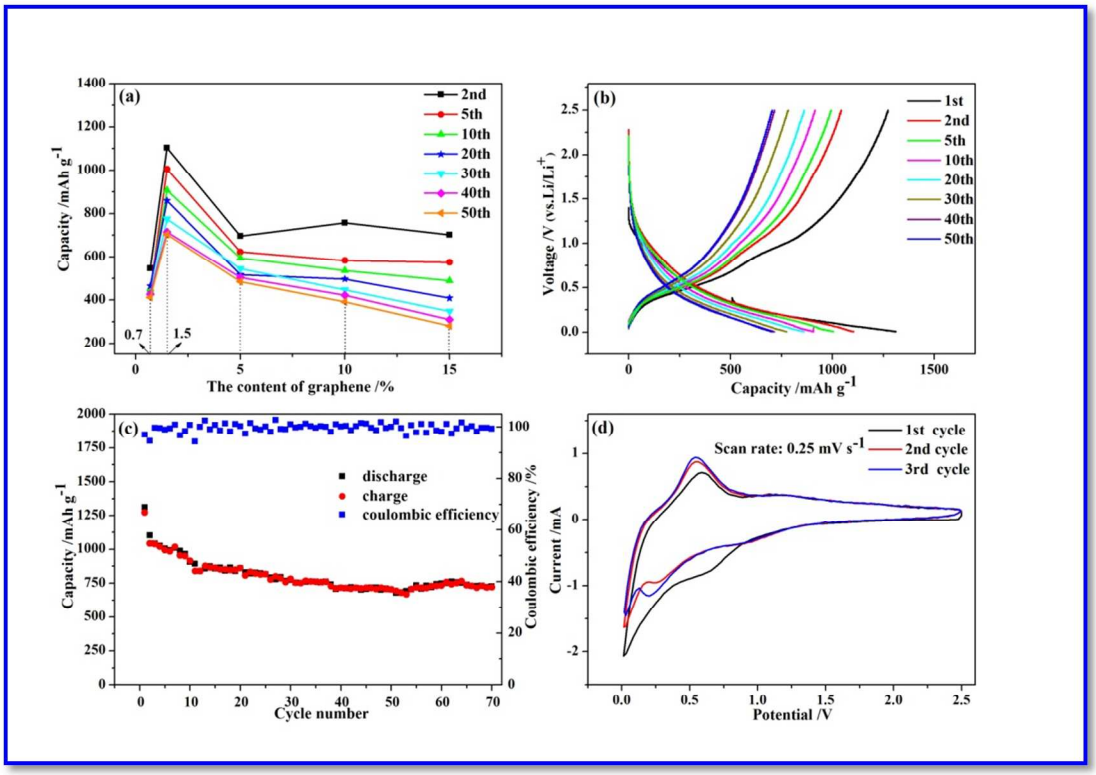

Fig. 7 (a) Specific capacity *vs.* graphene content, (b) the charge/discharge profiles of SnO_2/C/GN-1.5, (c) the cyclic performance of SnO_2/C/GN-1.5 and (d) the cyclic voltammograms of SnO_2/C/GN-1.5

The residual capacity between 20th to 30th circles is clearly shown in Fig. 6(b), the initial capacity loss are about 52%, 57%, and 66% for SnO_2/C-10, SnO_2/C-30 and SnO_2/C-50 after 30 cycles, respectively. Similar to a bulk SnO_2 system, the electrochemical curves of SnO_2/C show an extended plateau around 0.8 V in the first discharge, which is well known as the reaction of SnO_2 with lithium to form the solid electrolyte interface (SEI) layers.[23,37]

As shown in Fig. 6, all these three samples have a large and irreversible capacity, which is due to the formation of amorphous Li_2O matrix and the intense surface reactions between Li-Sn compounds and the electrolyte solution. It is well known that the rapid fading of SnO_2 electrode is mainly caused by a large volume expansion of SnO_2 occurring during the charge/discharge cycle, leading to the pulverization of the electrode. The improved electrochemical performance observed in our experiments should be attributed to the synergetic effect of SnO_2 and carbonaceous material. Carbonaceous material itself could store Li^+ and acts as electronic conductor. Furthermore, the carbonaceous material in SnO_2 based composites can limit the volume expansion during the process of lithium insertion.

In order to have a larger initial capacity and better retention of the reversible capacity for a long term cycling, SnO_2/C-50 with high initial capacity is used as starting material and is added GO before thermal treatment and then carbonized at 500°C. The resultant samples with varied GO contents are used as the anodes for LIBs.

Fig. 7(a) shows a comparison of the cyclic performances at a current density of 100 mA g^{-1} for SnO_2/C/GN-0.7, SnO_2/C/GN-1.5, SnO_2/C/GN-5, SnO_2/C/GN-10, and SnO_2/C/GN-15. For the 5th cycle, the capacities of all the five samples exhibit over 600 mAh g^{-1} except SnO_2/C/GO-0.7, which are much better than 565 mAh g^{-1} of SnO_2/C-50. SnO_2/C/GN-1.5 possesses the best cycling stability in all of the five samples, which is still above 720 mAh g^{-1} even after 70 cycles. The capacity retention of SnO_2/C/GN-1.5 after 30 cycles is about 70%, much higher than 34% of SnO_2/C-50 (see in Fig. 6(b)). This electrochemical improvement on SnO_2/C/GN is believed by the introduction of GN. The high surface area and excellent electrical conductivity of graphene not only afford the channels for electron transfer and the transport of electrolyte in carbon layer, but also help the formation and dispersion of SnO_2 NPs during carbonization, which also has been approved by XRD. Higher content of GN in SnO_2/C/GN not leads better electrochemical performance, which may be explained as follows. The conductivity of SnO_2/C/GN with 1.5 wt% GN is good enough for charge transfer during cycling. Meanwhile, the interactions between GN sheets are not strong as that between GN and PVA after thermal treatment. So, the higher loading of GN would weaken mechanical strength and render the easier pulverization of electrode during charge/discharge cycles.

In our experiments, SnO_2/C/GN-1.5 exhibits the best electrochemical performances as shown in Fig. 7(b). In the first cycle, SnO_2/C/GN-1.5 delivers a discharge capacity of 1312 mAh g^{-1} and a charge capacity of 1273 mAh g^{-1} at a current density of 100 mA g^{-1}. The coulombic efficiency of the first cycle is as high as 96%, much higher than 72% of SnO_2/C-50. The high coulombic efficiency of SnO_2/C/GN-1.5 is believed mainly resulting from the introduction of GN.[38] As shown in Fig. 7(c), the discharge capacity of

SnO_2/C/GN-1.5 is still up to 720 mAh g^{-1} after 70 cycles. SnO_2 NPs on graphene are found less aggregating into larger clusters, which might contribute the excellent cycling stability of SnO_2/C/GN-1.5. In order to better understand the reaction mechanism during charge/discharge cycles, cyclic voltammetry of SnO_2/C/GN-1.5 is given in Fig. 7(d). In the first cycle, the weak irreversible cathodic peak around 0.74 V is attributed to the formation of the solid electrolyte interface layer. This peak is not presented in the second cycle and afterwards. The clearly cathodic peak around 0.22 V and the anodic peak around 0.54 V are related to the lithium alloying reaction with Sn and dealloying of Li_xSn, respectively. The rate performance of SnO_2/C/GN-1.5 evaluated at various current densities is presented in Supporting Information (Fig. S5(a)). It is evident that the graphene framework has greatly improved the electron transfer and the stability of SnO_2/C/GN electrode compared to pure SnO_2 electrode. At a current density of 400 mA g^{-1}, SnO_2/C/GN-1.5 delivers a high capacity of 560 mAh g^{-1}, and rebounds back to 840 mAh g^{-1} when the current density swings back to 100 mA g^{-1}, which is still much higher than 372 mAh g^{-1} of the theoretical capacity of graphite.

The control experiments are carried out with pure SnO_2, C/GN and SnO_2/GN as the anode materials in LIBs at current rate of 100 mA g^{-1} under the same experimental conditions as those for SnO_2/C/GN. Fig. S5(b) shows the cycling performance of pure SnO_2, C/GN and SnO_2/GN, respectively. The capacities of the initial discharge/charge are 1219/599, 332/110 and 1391/704 mAh g^{-1}, respectively. After 35 cycles, the remaining capacities are 290, 81 and 565 mAh g^{-1}, which retain 23.8, 24.4 and 40.6%, respectively. The best electrochemical performance of above three samples belongs to SnO_2/GN, which is still much lower than that of SnO_2/C/GN-1.5. These data furthermore demonstrate that the C-PVA shell indeed has a great positive effect on the electrochemical stability of SnO_2.

4. Conclusions

A simple and effective protocol was presented to fabricate SnO_2/carbon/graphene nanocomposites with different compositions and nanostructures. PVA is selected as the cheap and ready available carbon source to form the supporting matrix for SnO_2 nanoparticles. The results show that the changes on the ratios of SnO_2 and graphene oxide can control the capacity of SnO_2/carbon/graphene. The improvement on the electrochemical performance of SnO_2/carbon/graphene can be achieved by "doping" certain amount of graphene. As ascribed to the synergetic effects of a unique combination of material properties, SnO_2/C/GN-1.5 with only 1.5 wt% GN shows a stable capacity at 720 mAh g^{-1} after 70 cycles, which uses much less GN in comparison to those in previous report. The planar graphene structure in SnO_2/C/GN could not only improve electrical conductivity, but also increase the crystallinity of SnO_2 and avoid particles agglomeration, which are beneficial for accommodating the large volume expansion and facilitating the electron transfer. The method described in this paper may provide a simple, economic and effective strategy for the preparation of metal-oxide/carbon/graphene composites.

Acknowledgements

This work was supported by the National Natural Science Foundation of China (Nos. 51303212, 51172285, 51372277); National Natural Science Foundation of Shandong Province (ZR2013EMQ013); The Fundamental Research Fund for the Central Universities (14CX02060A).

Notes and references

State Key Laboratory of Heavy Oil Processing, China University of Petroleum, Qingdao 266580, China. E-mail: wumb@upc.edu.cn.

*Corresponding author. Tel.:+86 532 8698 3452. E-mail address: wumb@upc.edu.cn

‡These authors contributed equally to this work.

† Electronic supplementary information (ESI) available.

1 Y. Idota, T. Kubota, A. Matsufuji, Y. Maekawa and T. Miyasaka, *Science*, 1997, **276**, 1395.
2 T. Nokami, T. Matsuo, Y. Inatomi, N. Hojo, T. Tsukagoshi, H. Yoshizawa, A. Shimizu, H. Kuramoto, K. Komae, H. Tsuyama and J. Yoshida, *J. Am. Chem. Soc.*, 2012, **134**, 19694.
3 B. Luo, B. Wang, M. H. Liang, J. Ning, X. L. Li and L. J. Zhi, *Adv. Mater.*, 2012, **24**, 1405.
4 J. R. Dahn, T. Zheng, Y. Liu and J. S. Xue, *Science*, 1995, **270**, 590.
5 A. Magasinski, P. Dixon, B. Hertzberg, A. Kvit, J. Ayala and G. Yushin, *Nat. Mater.*, 2010, **9**, 353.
6 A. M. Chockla, K. C. Klavetter, C. B. Mullins and B. A. Korgel, *Chem. Mater.*, 2012, **24**, 3738.
7 I. Kovalenko, B. Zdyrko, A. Magasinski, B. Hertzberg, Z. Milicev, R. Burtovyy, I. Luzinov and G.Yushin, *Science*, 2011, **333**, 75.
8 Y. L. Wang, T. Y. Wang, P. M. Da, M. Xu, H. Wu and G. F. Zheng, *Adv. Mater.*, 2013, **25,** 5177.
9 W. M. Zhang, J. S. Hu, Y. G. Guo, S. F. Zheng, L. S. Zhong, W. G. Song and L. J. Wan, *Adv. Mater.*, 2008, **20**, 1160.
10 R. Yang, Y. Gu, Y. Li, J. Zheng and X. Li, *Acta Mater.*, 2010, **58**, 866.
11 M. Winter and J. O. Besenhard, *Electrochim. Acta*, 1999, **45**, 31.
12 Y. Wang, J. Y. Lee and H. C. Zeng, *Chem. Mater.*, 2005, **17**, 3899.
13 M. S. Park, Y. M. Kang, G. X. Wang, S. X. Dou and H. K. Liu, *Adv. Funct. Mater.*, 2008, **18**, 455.
14 C. F. Zhang, X. Peng, Z. P. Guo, C. B. Cai, Z. X. Chen, D. Wexler, S. Li and H. K. Liu, *Carbon*, 2012, **50**, 1897.
15 J. W. Zhu, S. Chen, X. D. Wu, Q. F. Han and X. Wang, *ACS Nano*, 2010, **4**, 2822.
16 R. S. Ruoff, Y. W. Zhu, S. Murali, M. D. Stoller, K. J. Ganesh, W. W. Cai, P. J. Ferreira, A. Pirkle, R. M. Wallace, K. A. Cychosz, M. Thommes, D. Su and E. A. Stach, *Science*, 2011, **332**, 1537.
17 M. S. Park, Y. M. Kang, J. H. Kim, G. X. Wang, S. X. Dou, H. K. Liu, *Carbon*, 2008, **46**, 35.
18 R. Yang, W. Zhao, J. Zheng, X. Z. Zhang and X. G. Li, *J. Phys. Chem. C*, 2010, **114**, 20272.
19 Y. S. Jung, K. T. Lee and S. M. Oh, *Electrochim. Acta*, 2007, **52**, 7061.
20 X. W. Lou, C. M. Li and L. A. Archer, *Adv. Mater.*, 2009, **21**, 2536.
21 L. J. Fu, H. Liu, H. P. Zhang, C. Li, T. Zhang, Y. P. Wu, R. Holze and H. Q. Wu, *Electrochem. Commun.*, 2006, **8**, 1.
22 X. He, W. Pu, L. Wang, J. Ren, C. Jiang and C. Wan, *Solid State Ionics*, 2007, **178**, 833.
23 S. M. Paek, E. J. Yoo and I. Honma, *Nano Lett.*, 2009, **9**, 72.
24 J. Yao, X. P. Shen, B. Wang, H. K. Liu and G. X. Wang, *Electrochem. Commun.*, 2009, **11**, 1849.
25 D. Larcher, S. Beattie, M. Morcrette, K. Edstroem, J. C. Jumas and J. M. Tarascon, *J. Mater. Chem.*, 2007, **17**, 3759.

26 H. W. Song, N. Li, H. Cui and C. X. Wang, *J. Mater. Chem. A,* 2013, **1**, 7558.
27 X. S. Zhou, Y. X. Yin, L. J. Wan and Y. G. Guo, *J. Mater. Chem*., 2012, **22**, 17456.
28 G. Ji, B. Ding, Z. Sha, J. S. Wu, Y. Ma and J. Y. Lee, *Nanoscale*, 2013, **5**, 5965.
29 R. L. Liang, H. Q. Cao, D. Qian, J. X. Zhang and M. Z, Qu, *J. Mater. Chem*., 2011, **21**, 17654.
30 B. J. Li, H. Q. Cao, J. X. Zhang, M. Z, Qu, F. Lian and X. H. Kong, *J. Mater. Chem*., 2012, **22**, 2851.
31 C. F. Zhang, X. Peng, Z. P. Guo, C. B. Cai, Z. X. Chen, D. Wexler, S. Li and H. K. Liu, *Carbon*, 2012, **50**, 1897.
32 W. S. Hummers, R. E. Offeman, J. Am. Chem. Soc., 1958, **80**, 1339.
33 Y. X. Xu, K. X. Sheng, C. Li and G. Q. Shi, *ACS Nano*, 2010, **4**, 4324.
34 M. Zhang, D. N. Lei, Z. F. Du, X. M. Yin, L. B. Chen, Q. H. Li, Y. G. Wang and T. H. Wang, *J. Mater. Chem*., 2011, **21**, 1673.
35 R. Bissessur, P. K. Y. Liu, W. White and S. F. Scully, *Langmuir*, 2006, **22**, 1729.
36 J. Peckett, P. Trens, R. Gougeon, A. Poppl and R. Harris, *Carbon*, 2000, **38**, 345.
37 X. Sun, J. Liu and Y. Li, *Chem. Mater.*, 2006, **18**, 3486.
38 Q. Guo, Z. Zheng, H. L. Gao, J. Ma and X. Qin, *J. Power Sources*, 2013, **240**, 149.